Int. J. Nanoelectronics and Materials **5** (2012) 101-116

Comparative simulation of different nanoparticles concentration using a rectangular heat transfer micro tube

Fayadh M. Abed Al-Dulaimy [1,*] , Ghazi-Yousif- Mohammed Al-Shahery [2]

[1] *Mechanical Dept., College of Engineering, Tikrit University, Tikrit, Iraq*
[2] *Mechanical Dept., College of Engineering, Tikrit University, Tikrit, Iraq*

Received 10 Oct. 2011; Revised 11 Nov. 2011; Accepted 4 Dec. 2011

Abstract

Two nanofluids of γ-Al_2O_3 and Diamond with water base fluid used in rectangular micro channel heat exchanger with heat flux exposed from the bottom side. CFD Fluent is used for the flow calculations. For both nanofluids with grain size of less than 50 nm and concentrations of particles materials 1-5% is used. The Thermal conductivity, heat transfer coefficients, friction factor, pumping power, and pressure drop calculated for the flow ranging from 500 to 2000 Reynold number . The maximum Temperature attains in the channel at 60 ^oC for the heat flux of 100 w/cm^2 for diamond nanofluid and 80 ^oC for γ-Al_2O_3 nanofluid. The temperature reached above 100 ^OC for a heat flux of 200 w/cm^2 for both nanofluids.

Keywords: Nanofluid; Microchannel heat exchanger; Heat transfer enhancement.
PACS: 04.40.Nr; 88.40.me; 44.15.+a.

1. Introduction

Many ideas in conventional heat transfer presented to improve heat transfer either by the geometrical arrangement or including mixture of fluid. Since the last decade a demanding requirement for ultra-heat transfer become a need to cool electronic devices.
First is to find an optimum geometrical arrangement to extract heat generated from a high source of heat [1-5] and secondly to decrease the characteristic length which inversely increase the heat transfer coefficient [6]. For both the heat transfer coefficients and thermal conductivity found that to be enhancement.

The thermal conductivity of the coolant based not only on pure material but a new advantages being discovered that a nanofluids having to enhance thermal conductivity by fourfold over conventional fluids, while nanofluids are mixture of nano particles of selective materials into a base fluids [7-13].

The optimum particles size is only effective shown experimentally with less than 50 nm grain size independent of the materials, which reasoned to the surface area of the particles dispersed in the base fluids. There is a marked increase with respect to particles thermal conductivity in relation to its intrinsic properties such variation noticed for AL_2O_3, cu, and diamond, respectively [14].

[*]) For correspondence, Tel: + (064) 7702597719, E-mail: fayadh_mohamed@yahoo.com

Consequently, there is an increased need for utilization of a variety of duct geometries for heat transfer applications with forced convection and internal flow shows efficiently improved [15], due to the size and volume constraints in applications, such as aerospace, nuclear, biomedical engineering, and electronics, the utilization of non-circular flow passage geometries are required, particularly, with respect to compact heat exchangers duct [15]. Many investigators optimized results for different geometries related to heat transfer enhancement which indicates that the triangular and the square cross have marginally better than that of the circular cross section [14].

Shah [16] and Shah and London [17] studied the heat transfer characteristics of laminar flow in a wide variety of channel shapes, including equilateral triangular, equilateral triangular with rounded corners, isosceles triangular, right triangular, and arbitrary triangular cross-sectional ducts, for an extensive range of thermal boundary conditions. Furthermore, Gupta et al. [18] studied fully developed laminar flow and heat transfer in equilateral triangular cross-sectional ducts with constant heat flux.

Limited studies regarding the use nanofluids as coolants in micro and minichannel heat sinks exist in literature. Nguyen et al. [19] have investigated the usage of nanofluids in cooling electronic devices with nanofluids as the coolant marked reduction in the junction temperature was observed, especially at higher flow rates and higher particle loading percentage.

For more than a decade, investigations have been conducted research for better understanding of fluid flow and heat transfer characteristics in silicon-based microchannel heat sinks designed for applications in electronic cooling. It is important to note that in silicon-based MEMS technology, unlike larger-scale conventional heat exchangers, microchannels are fabricated as an integral part of silicon wafers, often with noncircular cross-sections due to the fabrication processes used, i.e., trapezoidal, triangular or rectangular. The cross-sectional shape of a channel can have a significant influence on the fluid flow and heat transfer characteristics in noncircular microchannels. Typically, a coolant is forced through a large number of parallel channels, which are in contact with a hot surface, to convect evolved heat away and provide a near-uniform temperature field in the device to be cooled. Micro channel cooling is a promising way to solve the cooling problem for computer chips. In micro channel cooling a fluid is flowing through a micro channel in close contact with the electronic chips. Due to the large area to volume ratio of the micro channel, the heat removal is larger than by conventional air cooling. Heat transfer by forced convection for gases is in the range 25-250 kw/m^2[20], whereas experimental micro channels with water have shown a heat flux of 500 kw/m^2 [21]. The aim of this work is to study the heat transfer enhancement for two nano materials with water of distinct intrinsic thermal properties in a rectangular microchannel that exposed to different heat flux range up to un ultimate heat that give surface temperature of near 80 degree. The fluid flow variation from 500 to 2000 Reynold number also considered as to show its effectiveness in heat transfer.

2. Governing equations

In order to examine the impact of various nanofluids utilization on the MCHS cooling performance, the following assumptions are made:(i) both fluid flow and heat transfer are in steady-state and three dimensional flow; (ii) fluid is in a single phase, incompressible with laminar flow; (iii) all the surfaces of heat sink exposed to the surroundings are assumed to be insulated except the bottom of the microchannel heat sink exposed to constant heat flux. The continuity, momentum and energy equations [12], for the current problem with an assumption of steady laminar, and incompressible flow conditions

together with the specified boundary conditions, are solved using the finite volume based computational fluid dynamics solver FLUENT 12.0 [10]. The second order upwind scheme is used for the analysis. The equations are used for this 3-D laminar incompressible flow analysis are:

$$\frac{\partial u}{\partial x}+\frac{\partial v}{\partial y}+\frac{\partial w}{\partial z}=0 \tag{1}$$

$$\left.\begin{aligned}\rho\left(u\frac{\partial u}{\partial x}+v\frac{\partial u}{\partial y}+w\frac{\partial u}{\partial z}\right)&=-\frac{\partial p}{\partial x}+\mu\left(\frac{\partial^2 u}{\partial x^2}+\frac{\partial^2 u}{\partial y^2}+\frac{\partial^2 u}{\partial z^2}\right)\\ \rho\left(u\frac{\partial v}{\partial x}+v\frac{\partial v}{\partial y}+w\frac{\partial v}{\partial z}\right)&=-\frac{\partial p}{\partial y}+\mu\left(\frac{\partial^2 v}{\partial x^2}+\frac{\partial^2 v}{\partial y^2}+\frac{\partial^2 v}{\partial z^2}\right)\\ \rho\left(u\frac{\partial w}{\partial x}+v\frac{\partial w}{\partial y}+w\frac{\partial w}{\partial z}\right)&=-\frac{\partial p}{\partial z}+\mu\left(\frac{\partial^2 w}{\partial x^2}+\frac{\partial^2 w}{\partial y^2}+\frac{\partial^2 w}{\partial z^2}\right)\end{aligned}\right\} \tag{2}$$

$$\rho C_p\left(u\frac{\partial T_f}{\partial x}+v\frac{\partial T_f}{\partial y}+w\frac{\partial T_f}{\partial z}\right)=K_{nf}\left(\frac{\partial^2 T_f}{\partial x^2}+\frac{\partial^2 T_f}{\partial y^2}+\frac{\partial^2 T_f}{\partial z^2}\right) \tag{3}$$

$$\frac{\partial}{\partial x}\left(K_p\frac{\partial T_p}{\partial x}\right)+\frac{\partial}{\partial y}\left(K_p\frac{\partial T_p}{\partial y}\right)+\frac{\partial}{\partial z}\left(K_p\frac{\partial T_p}{\partial z}\right)=0 \tag{4}$$

3. Mathematical formulation

3.1. MCHS model

The physical configuration of MCHS (Micro Channel Heat Sink) is schematically shown in Figure. 1. The heat supplied to the bottom plate is removed by flowing fluid through a number of microchannels. The thermophysical properties for the types of nanoparticles, base fluid (water), and the nanofluids with particle volume fraction of 0, 1%, 3%and 5% are listed in Table 1. For the two types of nanofluids,(γ-Al_2O_3 and Diamond with H_2O), the density, thermal conductivity, and dynamic viscosity appear significantly higher that the pure water (13%,11%), (12.8%,20%) and (20%, 18%) respectively, while the specific heat of nanofluids is lower with a relative decrease of (3.5%, 13%).

Table 1: Thermal physical properties of nanofluid at 293 ^{0}K.

Nanofluid	Al_2O_3- water				Diamond -Water			
Φ	ρ_{nf}	$(Cp)_{nf}$	μ_{nf}	k_{nf}	ρ_{nf}	$(Cp)_{nf}$	μ_{nf}	k_{nf}
0.00	998	4147.	0.0010	0.5970	998	4181.8	0.0010	0.5970
0.010	1030.21	4113.5	0.0011	0.6134	1023.3	4055.6	0.00108	0.63797
0.030	1089.60	4045.2	0.0013	0.6484	1073.5	3820.58	0.00113	0.69110
0.050	1148.99	4011.2	0.0017	0.6856	1123.79	3606.56	0.00119	0.74894

3.2 Physical Model

A micro-channel heat sink usually consists of a number of identical channels. Numerical simulation of the entire unit needs large amount of CPU time. A schematic diagram of the proposed micro-channel heat sink is shown in Figure. 1. The geometry consists of a rectangular channel 230 μm (Width) X 230 μm (Height) in cross-section, and 10 mm (Length) in length. A uniform heat flux of 100,200 and 250 W/cm^2 are applied at the bottom surface of heat sink whereas the other sides adiabatic boundary conditions are applied. As a hydraulic boundary conditions, a uniform velocity is applied at the channel inlet, the velocity in x and y direction are zero and velocity in z direction is calculated depends on the selected value of Re, hydraulic diameter and properties of nanofluid. The fluid inlet temperature is specified in the inlet region while at the exit, pressure was specified.

3.3 Geometry and preprocessing

The computational domain, meshing, labeling boundary conditions were created in the commercial pre-processor software GAMBIT 2.3.16 as shown in Figure.1. Three different meshes, 1×10^5, 2×10^5, and 4×10^5 tested and compared in terms of the heat transfer coefficient. It is found that mesh number of around 2×10^5 gives about 1% deviation compared to mesh size of 4×10^5; whereas the results from mesh number of 1×10^5 deviate by up to 8% compared to those from the finest one. Therefore, a mesh of around 2×10^5 ($20 \times 20 \times 500$) elements was considered sufficient for the numerical investigation purposes.

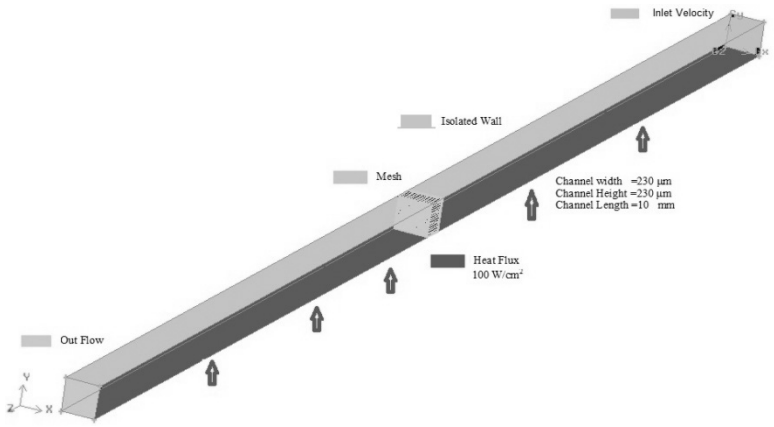

Fig. 1: Schematic Diagram of the Micro-channel Heat Sink.

3.4 Solver criterion

The CFD method follows the use of commercial software ANSYS Fluent 12.0 to solve the problem. The specified solver in Fluent uses a pressure correction based iterative SIMPLE algorithm with second order upwind scheme for discretizing the convective transport terms. The convergence criteria for all the dependent variables are specified as

0.00001. The values of under-relaxation factor found to be most suitable are shown in Table 2.

Table 2: Relaxation Factor

Variables	Pressure	Density	Momentum	Energy
Values	0.3	1.0	0.08	1.0

3.5 Thermo-physical properties of base- nano fluids and nanoparticles

The base-fluid considered in this work is water. Thermo-physical properties were obtained as polynomial functions of temperature found some were else [**22]** as:

$$\rho_w = -3.57\times10^{-3}T^2 + 1.88T + 753.2 \quad (5)$$

while the water viscosity is given by

$$\mu_w = 2.591\times10^{-5}\times10^{238.3/(T-143.2)} \quad (6)$$

and the thermal conductivity of water is calculated from

$$K_w = -8.354\times10^{-6}T^2 + 6.53\times10^{-3}T - 0.5981 \quad (7)$$

The specific heat of water is considered constant at $Cp_w = 4200$. The physical properties of the base fluid and nanoparticles are shown in Table.3

Table 3: Physical properties of base fluid water, alumina and Diamond at 20°C (293 K)

Material	ρ (Kg /m^3)	Cp (J /Kg.K)	k (W /m.K)	μ (Ns/m^2)
Water	998	4181.8	0.597	0.001003
γ-Al_2O_3	3880	773	36	
Diamond	3510	497.26	1000	

3.6 Nanofluids Thermal properties.

In mixing the nanoparticles with base fluid in the concentration used for this study, as for the nano fluid density and specific heat estimated in the following relationship.

$$\rho_{nf} = (1-\phi)\rho_{bf} + \phi\rho_p \quad (8)$$

$$(Cp)_{bf} = \frac{(1-\phi)(\rho Cp)_{bf} + \phi(\rho Cp)_p}{(1-\phi)\rho_{bf} + \phi\rho_p} \text{[23].} \quad (9)$$

For the viscosity Enstein [24] expression is used in determine the dynamic viscosity for particles in diluted fluid which is $\mu_{nf} = \mu_{bf}(1+2.5\phi)$ for $\phi < 5\%$. But other used different relations for larger particles size [19], $\mu_{nf} = \mu_{bf}(150\phi^2 + 2.5\phi + 1)$ and (Maiga et

al., 2004) [25] has used modified experimental fitted data to takes account of interaction of particles and the fluid for Al_2O_3-Water nanofluids. $\mu_{nf} = \mu_{bf}\left(123\phi^2 + 7.3\phi + 1\right)$. The Diamond –water nanofluids are estimated and given in table.1 these parameters are of equation 8 and 9 and 10 for density, specific heat and dynamic viscosity respectively, but the thermal conductivity are estimated graphically from Figure 2.

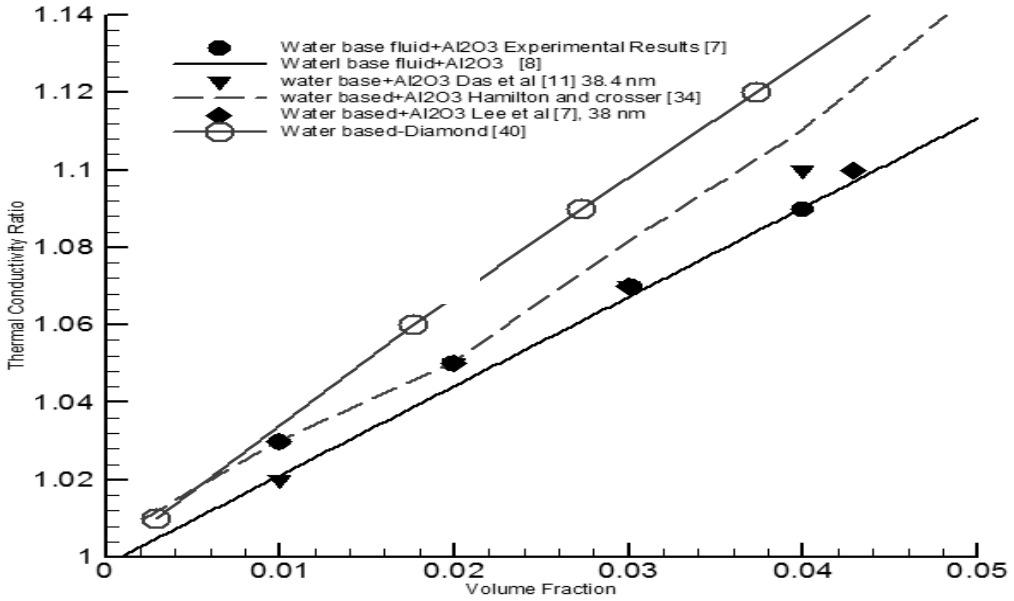

Fig. 2: Experimental data for nanofluids (γ - Al2O3 and diamond with water based fluid).

3.7 Thermal Conductivity

Theoretical model influenced thermal conductivity of nanofluid. Many investigator since Maxwell model[27] for thermal conductivity of suspended solid/liquid in the micro and macro scale size particles cannot explain fully the nanofluids behavior but it can be assumed as for the static mode of the thermal conductivity of nonofluids. Only recently other investigators used Both the Maxwell static thermal conductivity and the dynamic Brownians and Enstien random motion are effective contributors, but The Brownian motion mean free path is far shorter than that the diffusion length of stoke Enstien [24] which is the dominant parameter in heat distribution in nanofluid.

In a nanoparticles mixture dependence founds to have good heat transfer characteristics related to particles size and has been found that the enhancement are at maximum of 50 nm grain size and for larger sizes give a study state Figure 3.

Figure 4 shows the dynamic Brownian motions contribution while it is shown constant as related to Maxwell model. The classical Maxwell model [27] For solid liquid mixtures, for relatively large particles size macro and mille metric sizes is good for low solid concentration Bruggeman (1935) [33] proposed a model depending on the Maxwell with modification of shape factor and Hamilton and Crosser (1962) [34] introduced the shape factor to account the effect the shape of the particles which reveals that Maxwell's model is a special case of Hamilton and Crosser's model for sphericity equal to one.

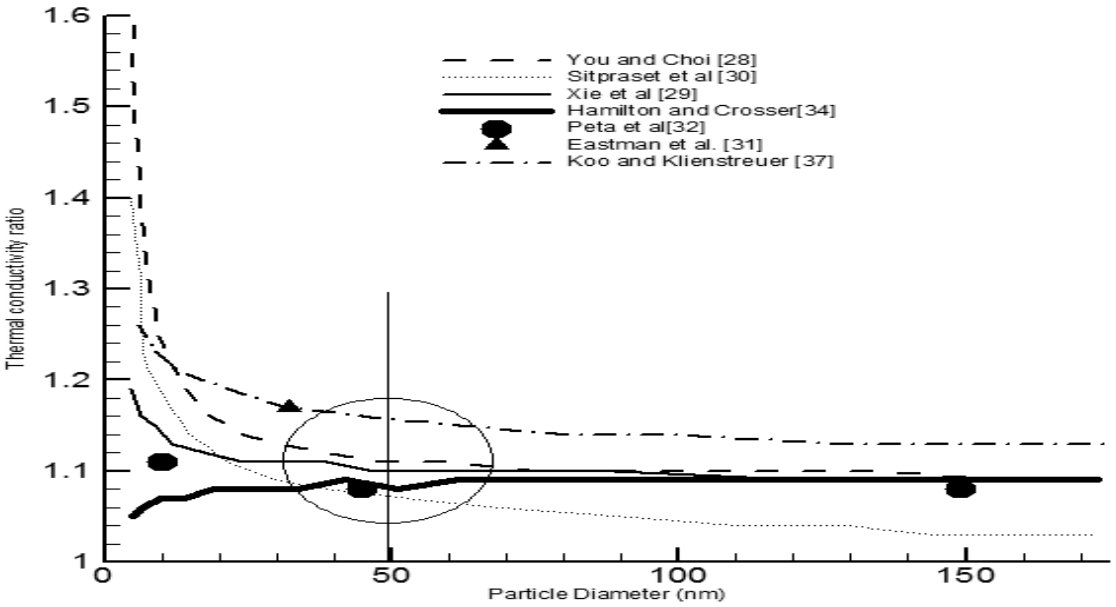

Fig. 3: Comparison of the experimental results of the thermal conductivity ratio for 3 vol. % (γ-Al_2O_3)-water nanofluid with theoretical models as a function of particle size.

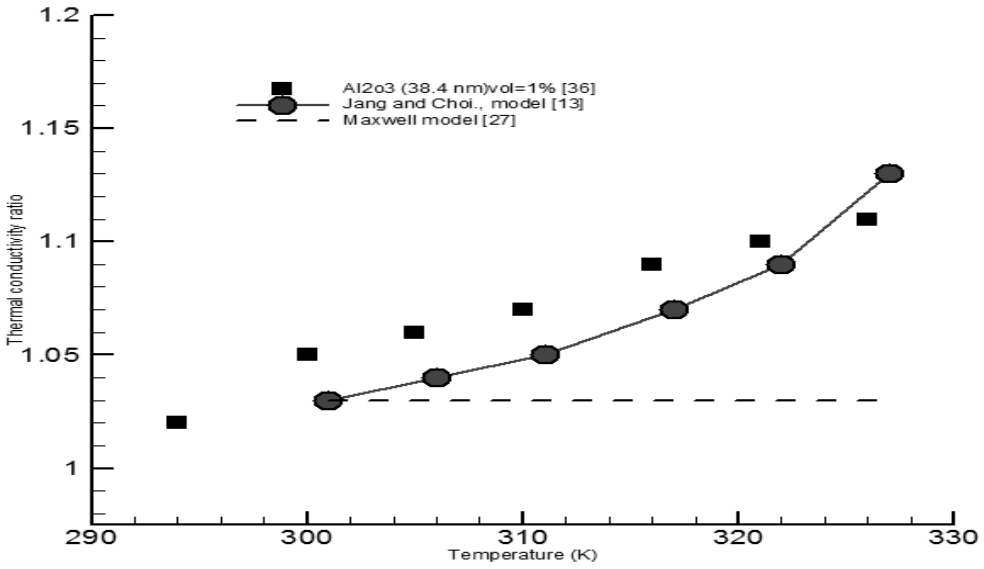

Fig. 4: Experimental data for temperature-dependent conductivity and the Maxwell model.

The thermal conductivity of the present nanofluid increment with temperature by up to fourfold over a small temperature range (20–50°C) Das et al. [35]. This phenomenon cannot be explained by classical models such as the Maxwell model [27] as shown in Figure. 4.

To explain this deviation the Brownian motion of nanoparticles in nonofluid expressed well in Brownian motion suggested by Enstien [24]. The calculation carried out by the following equation:

$$K_{nf} = k_{bf}(1-\phi) + \beta k_{particle}\phi + C_1 \frac{d_{\mathrm{bf}}}{d_{nono}} \mathrm{k_{bf}} \mathrm{Re}^2_{d_{nano}} \ \mathrm{Pr}\varphi \quad \mathrm{Re}_{d_{nano}} = \frac{\mathrm{C_{R.M}} d_{nano}}{\nu}, \ \mathrm{C_{R.M}} = \frac{\mathrm{D_0}}{L_{bf}},$$

$Where\, \mathrm{C}_1 = 7.2\times10^7$ for water

The used model is that of Chon et al. [36] empirical correlation of nano fluid due to its extensive range in terms of particles size and temperature:

$$\frac{k_{nf}}{k_{bf}} = 1 + 64.7\phi^{0.7460}\left(\frac{d_{bf}}{d_p}\right)^{0.3690}\left(\frac{k_p}{k_{bf}}\right)^{0.7476} \mathrm{Pr}^{0.9955}\,\mathrm{Re}^{1.2321}$$

Here, Prandtl number and Reynolds number are defined as follows $\mathrm{Pr} = \frac{\mu_{bf}}{\rho_{bf}\alpha_{bf}}$, $\mathrm{Re} = \frac{\rho_{bf} V_{br} d_p}{\mu_{bf}}$ and V_{br} is calculated by using the following expression $V_{br} = \frac{K_B T}{3\pi\mu_{bf} d_p \lambda_{bf}}$,were L_{bf} : Mean free path for water=0.738 (nm) and 35 (nm) for Al_2O_3 ans β is constant for considering the Kapitza resistance per unit area.= 0.01.

3.8 Pure and nanofluid temperature.

In the system being considered, the energy generated by the exposed heat flux on the bottom of MCHS is absorbed by the working fluid. The nanofluid- and pure fluid-cooling MCHS, then energy absorbed by the working fluid can be written as,

$$Q_{nf} = (\rho Cp)_{nf} \dot{V}_{nf} (T_{nfo} - T_{nfi}) = (\rho Cp)_{nf} \dot{V}_{nf} \Delta T_{nf},$$

$$Q_f = (\rho Cp)_f \dot{V}_f (T_{fo} - T_{fi}) = (\rho Cp)_f \dot{V}_f \Delta T_f,$$

noting that the thermal capacity of the nanofluid is usually smaller than that for the pure fluid because of the low specific heat of nanoparticles. From Newton's law of cooling, the local heat transfer coefficient for both nanofluid- and pure fluid-cooled MCHS can be written as $q'' = h_{nf}(x)\left(T_{snf}(x) - T_{nf}(x)\right) = h_f(x)\left(T_{sf}(x) - T_f(x)\right)$,

$$h_{nf}(x) = \frac{q''}{\left(T_{snf}(x) - T_{nf}(x)\right)}, h_f(x) = \frac{q''}{\left(T_{sf}(x) - T_f(x)\right)},$$

in order to established a heat transfer enhancement by the nanofluid If the , $h_{nf}(x) > h_f(x)$ and $Q_{nf} > Q_f$ conditionally $\dot{V}_{nf} = \dot{V}_f$ and $T_{nfi} = T_{fi}$, we observed that

$$(T_{nfo} - T_{nfi}) > (T_{fo} - T_{fi}) \tag{10}$$

$$(T_{snf}(x) - T_{nf}(x)) < (T_{sf}(x) - T_f(x)) \tag{11}$$

by Combining Eqs. (10) and (11), it can be found that

$$T_{snf}(x) < T_{sf}(x) \tag{12}$$

This result indicates that nanofluid-can cool MCHS better that pure fluid.

4. Results and discussion

In order to distinguished the various effect of nanofluid behavior a single choice of rectangular tube geometry for a specified well established nanoparticles concentration for two well-known materials that is the gamma alumina and diamond, the choice of these types of particles due to its role with fluid.

In order to eliminate the surface interaction between particles and fluid one is diamond, which is completely inert with water only surface adhesion can be accounted for. However, alumina surface adherence to water is different from diamond whatever inertness it possesses. From some of the estimated results, for the same flow conditions, the friction factor it appears nearly constant for different concentration from diamond while for alumina it has linearly changing with the flow. This mean that the water adhesion or some surface reactivity differed from that of diamond which indicates clearly that water adhere to alumina surface causing larger apparent size then a drag effectively contribute to a more pumping power as shown in Figure 5.

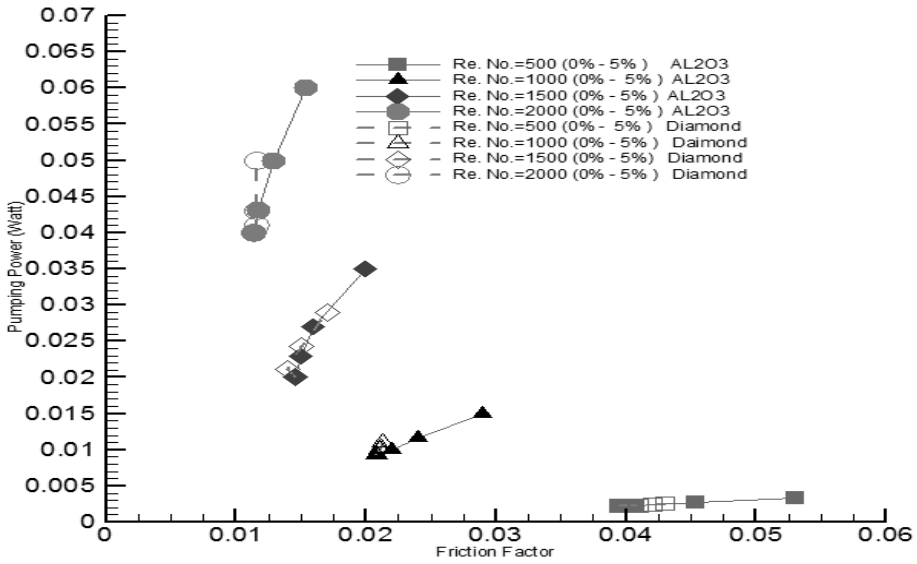

Fig. 5: Pumping power- Friction Factor relationship of Micro-channel heat sink with water, water is the base fluid with γ -AL_2O_3 and Diamond nanoparticles.

Despite that both nanoparticles shared enhancement of heat transfer with a good thermal conductance from the wall of the microchannel Figure (6 and 7). On the other hand the thermal resistance behavior are inversely proportional to pumping power while the thermal friction factor is directly proportional to pumping power Figure (5 and 8) respectively.

Moreover the diamond nanofluid having almost a friction less behavior for a specific flow conditions, only for low flow rate (RE=500) of diamond nanofluid a sedimentation effect appears as shown in Figure (8). Also it confirms this result from pressure drop Figure. 9 then the water diamond adhesion solely effective as far as the pressure drop linearly changing with the volume fraction. The same contribution appears for the friction factor and particles volume fraction as shown in Figure (10).

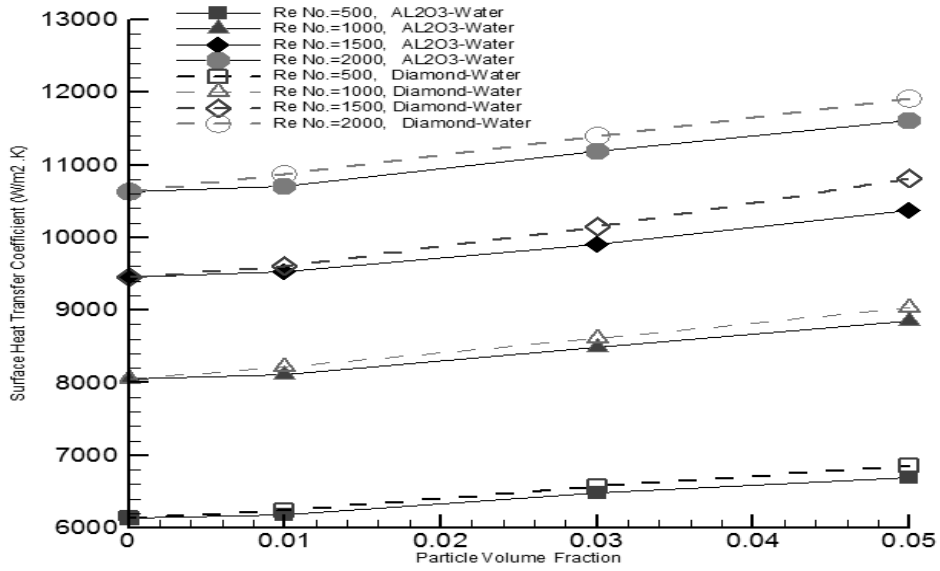

Fig. 6: Effect of Surface Heat Transfer Coefficient versus volume of fraction of (Diamond and Al_2O3-water) for different flow velocity.

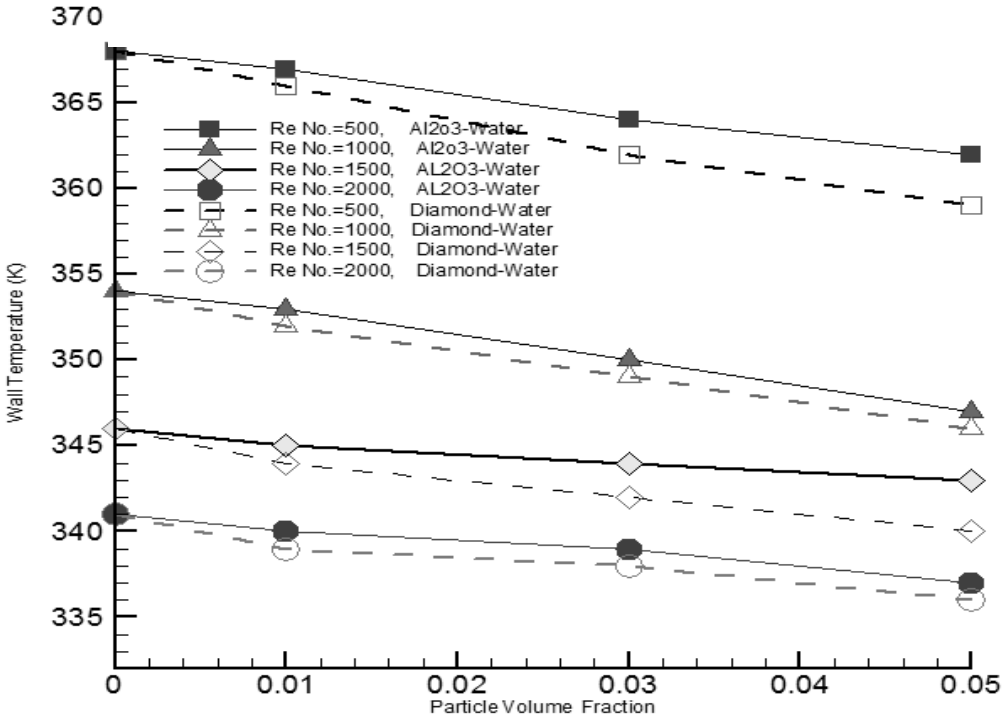

Fig. 7: Variation of Wall Temperature versus volume of fraction of (Diamond and Al2o3-water) for different flow velocity.

Moreover the diamond nanofluid having almost a friction less behavior for a specific flow conditions, only for low flow rate (RE=500) of diamond nanofluid a sedimentation effect appears as shown in Figure (8). Also it confirms this result from pressure drop Figure. 9 then the water diamond adhesion solely effective as far as the pressure drop linearly changing with the volume fraction. The same contribution appears for the friction factor and particles volume fraction as shown in Figure (10).

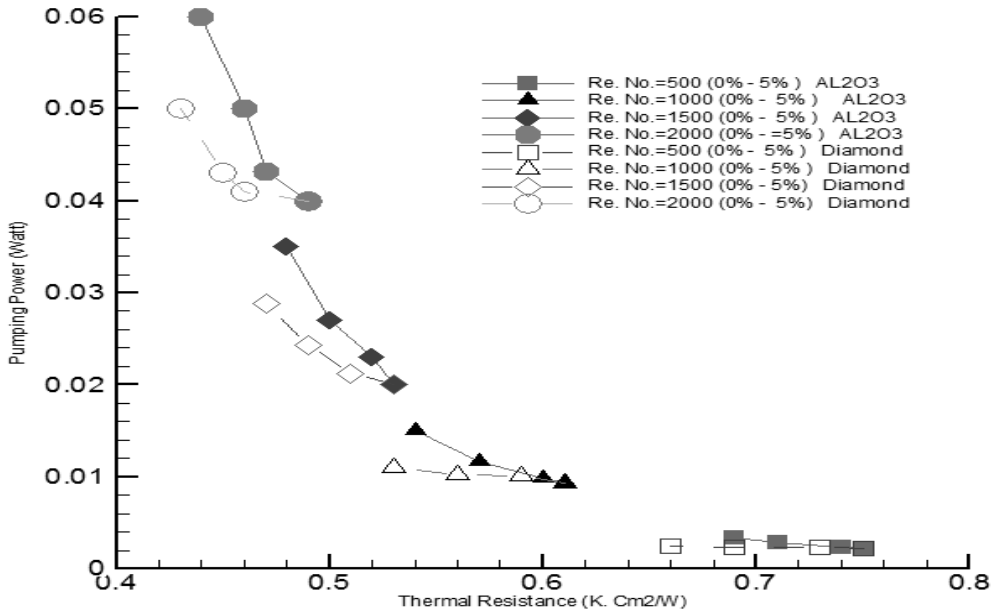

Fig. 8: Thermal Resistances of Microchannel heat sink with water, water is the base fluid with γ- AL_2O_3 and Diamond nanoparticles

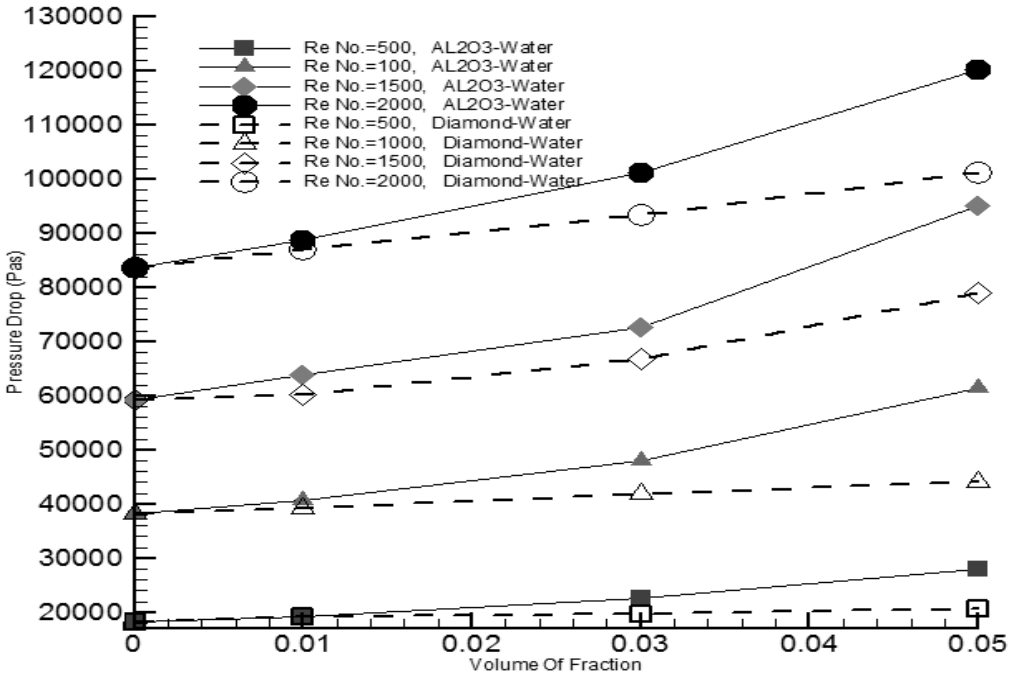

Fig. 9: Variation of Pressure Drop versus volume of fraction of (Diamond and Al2o3-water) for different flow velocity.

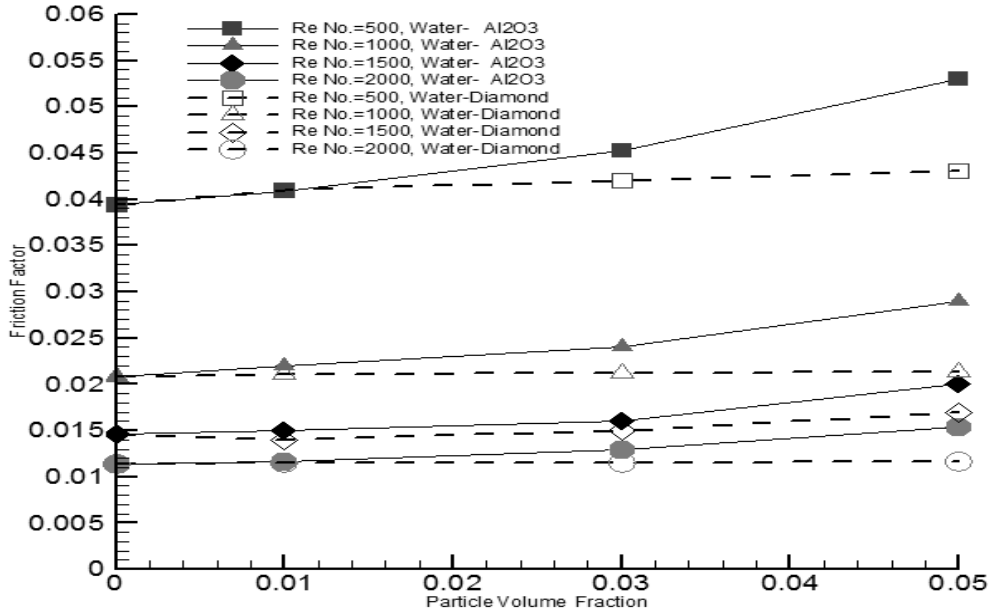

Fig. 10: Variation of Friction factor versus particles volume fraction of (Diamond and γ - Al_2O_3-Water) for different flow velocity

From Figure 11 it is complementary evidence to what has obtained that the pumping power linearly increasing with the volume fraction for the diamond but a slight nonlinear increment for γ-AL_2O_3 which is related to the previously mentioned behavior. The conclusive result is that the thermal resistance with the volume fraction have a linear changing with the volume fraction is an indicative to the value of the thermal conduction enhancement as shown in Figure 12.

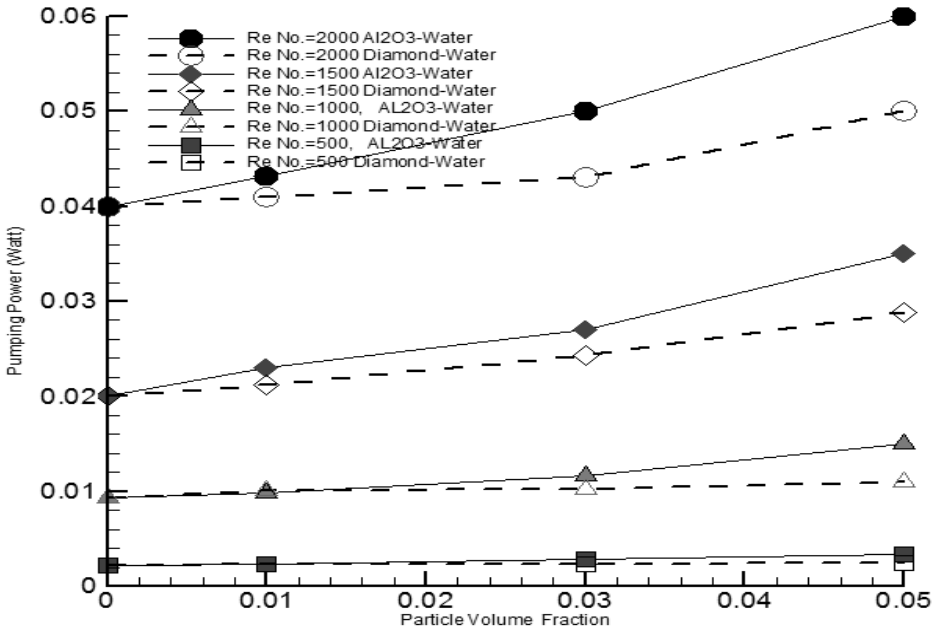

Fig. 11: Variation Pumping Power versus volume of fraction of (Diamond and γ- AL_2O_3-Water) for different flow velocity.

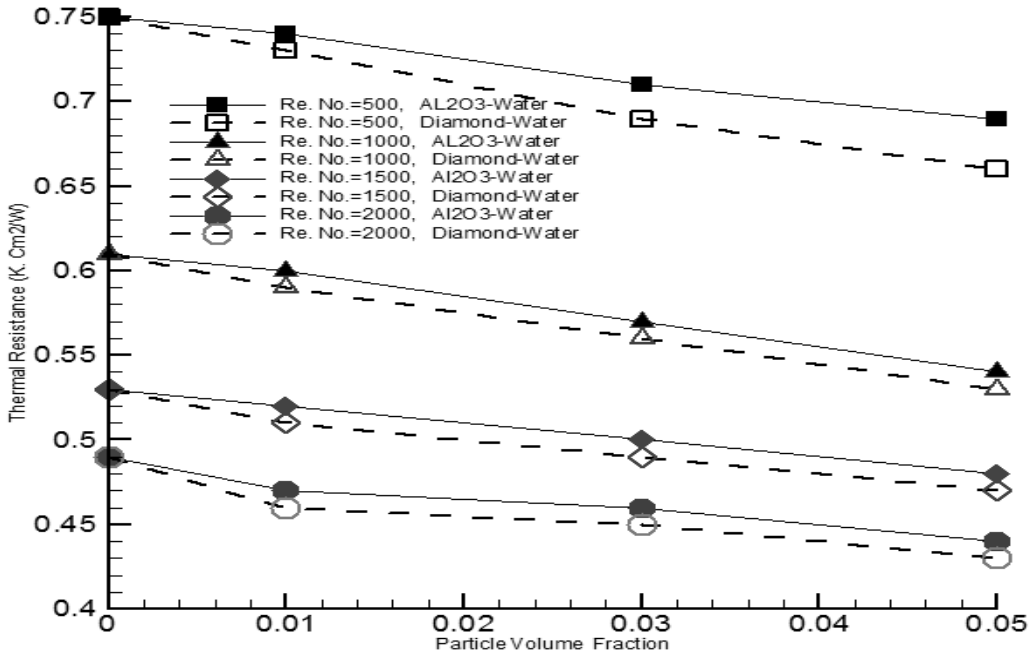

Fig. 12: Thermal Resistances of Microchannel heat sink with water, water is the base fluid with (Diamond and γ- AL_2O_3) nanoparticles.

The obtained results were carried out by numerical simulation on rectangular tube geometry, for two nanofluid types with four concentrations each. The velocity characterized the flow from 500 to 2000 Reynold number. On these conditions of nanofluid types, concentrations and flow the bottom heat flux exposed to microchannel of 100 and 200 W/cm^2, found to be at the 200 W/cm^2 a high temperature ranging above 100 ^0C. Due to this result it limits this configuration to a 100 w/cm^2 to be a useable value.

In conclusion graphing of pumping power flow and temperature are given in fig 13 and 14. From these results an equilibrium characterized the flow between 1000 and 1500 Reynold number for an attained temperature of (40 -60 ^0C) for diamond and the temperature reached for a Lumina nanofluid reached (60-80 ^0C)

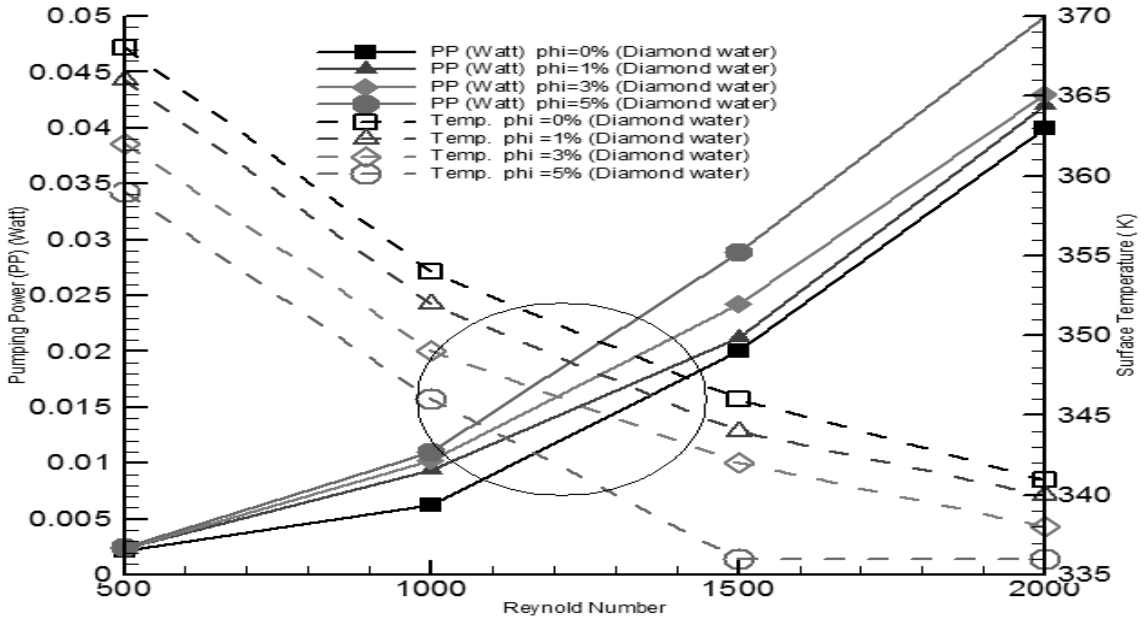

Fig. 13: Pumping Power Flow-Temperature Diagram for Diamond-nanofluid at heat flux of 100 W/cm2.

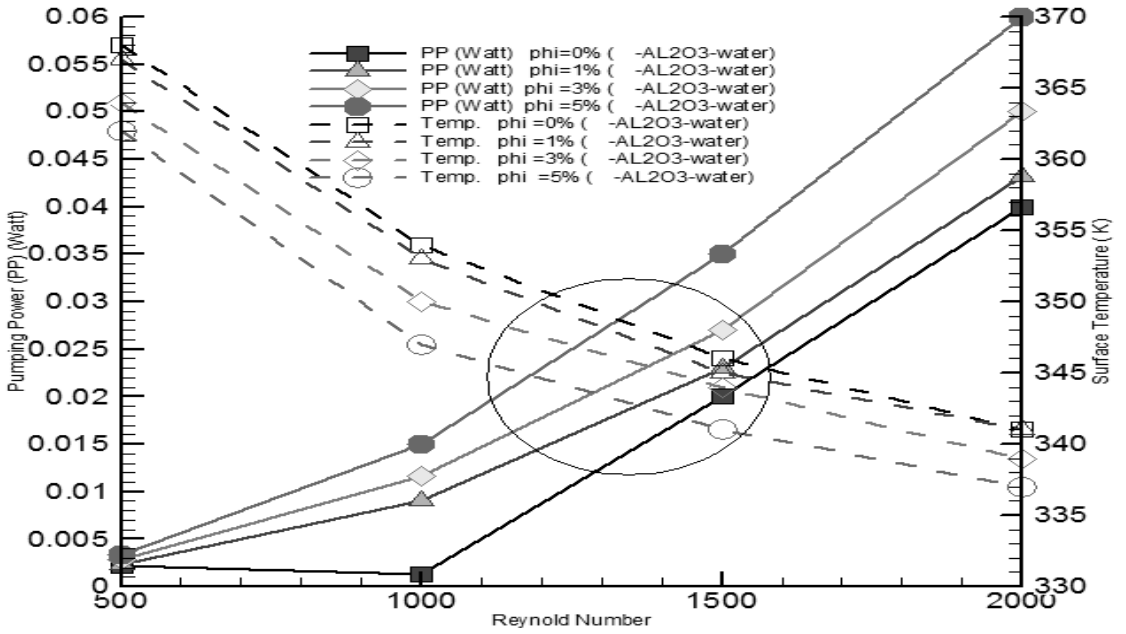

Fig. 14: Pumping Power Flow-Temperature Diagram for γ -AL2O3-nanofluid at heat flux of 100 W/cm2.

5. Conclusion

The simulated flow inside a rectangular micro channel for the two nanofluids mainly γ-Al_2O_3 and Diamond with water base to conduct heat flux exposed from bottom side of the channel to be constant at 100 w/cm^2 and 200 w/cm^2.

The flow of the fluid assumed laminar in range of 500 to 2000 Reynold numbers, for both nanofluid having concentration of 1%, 3% and 5%.

The obtained results that the added nanoparticles to water base fluid increased the friction factor, also an increasing in surface heat transfer coefficient with both concentration of nanoparticles, however for diamond nanofluid a higher transfer coefficient than that of alumina which also reflect the better conductivity of diamond than γ-Al_2O_3 in term of its intrinsic thermal properties.

Both nanofluid the thermal resistance decreased with increasing concentrations which the friction factor increasing with direct proportionality to the concentration.
The wall temperature attained for both nanofluid having maximum 60 ^{0}C for diamond and at a maximum of 80 ^{0}C for alumina nanofluids.

It is of interest to see experimental result for Borazone nanoparticles (Cubic BN) with fombileen fluid in order to see the effect with no surface interaction and less friction coefficient.

References

[1] D. B. Tuckerman, R. F. W. Pease, IEEE Electron Dev. Lett. **2** (1981) 126
[2] A. Goyal, R.C. Jaeger, S. H. Bhavnani, C. D. Ellis, N. K. Phadke, M. Azimi-Rashti, J. S. Goodling, IEEE Electron Dev. Lett. **14** (1993) 29
[3] S. P. Jang, S. J. Kim, K. W. Paik, Sens. Actuators A **105** (2003) 211
[4] X. Wei, Y. Joshi, IEEE Trans. Comp. Packag. Manufact. Technol. **26** (2003) 55
[5] J. Y. Min, S. P. Jang, S. J. Kim, Int. J. Heat Mass Transfer **47** (2004) 1099
[6] Y. S. Muzychka, International Journal of Heat and Mass Transfer **48** (2005) 3119
[7] S. Lee, S. U. S. Choi, J. A. Eastman, ASME J. Heat Mass Transfer **121** (1999) 280
[8] J. A. Eastman, S. U. S. Choi, S. Li, W. Yu, L.J. Thompson, Appl. Phys. Lett. **78** (2001) 718
[9] S. U. S. Choi, Z.G. Zhang, W. Yu, F. E. Lockwood, E. A. Grulke, Appl. Phys. Lett. **79** (2001) 2252
[10] S. K. Das, N. Putta, P. Thiesen, W. Roetzel, ASME J. Heat Transfer **125** (2003) 567
[11] H. E. Patel, S.K. Das, T. Sundararajan, A.S. Nair, B. George, T. Pradeep, Appl. Phys. Lett. **83** (2003) 2931
[12] D. H. Kumar, H. E. Patel, V. R. R. Kumar, T. Sundararajan, T. Pradeep, S.K. Das,Phys. Rev. Lett. **93** (2004) 144301
[13] S. P. Jang, S. U. S. Choi, Appl. Phys. Lett. **84** (2004) 4316
[14] S. P. Jang, S. U. S. Choi, Applied Thermal Engineering **26** (2006) 2457
[15] Sahin AZ, Energy, **23**, 6 (1998) 465
[16] Shah R. K, Int. J. Heat Mass Transf. **18** (1975) 849
[17] Shah R. K, London A. L. *Laminar Flow Forced Convection in Ducts,* New York: Academic Press Inc (1978)
[18] Gupta R.V., Geyer P.E., Fletcher D.F., Haynes B.S., Int. J. Heat Mass Transf. **51** (2008) 2925
[19] Nguyen, C., Desgranges, F., Roy, G., Galanis, N., Maré, T., Boucher, S., Angue Mintsa, H., Int. J. Heat Fluid Fl., **28** 6 (2007) 1492
[20] Incropera, F. P., De Witt, D. F, *Fundamentals of heat and mass transfer*, Wiley (2001)
[21] Kuan, W. K., Kandlikar, S. G., Journal of heat transfer, **130** (2008) 034503
[22] Kays W., Crawford M., Weigand B., *Convective Heat and Mass Transport*. 4 Edition. Singapore, MacGraw Hill, (2005)

[23] Yang, Y., Zhang, Z. G.,Grulke, E. A., Anderson, W. B., Wu, G. F., Int. J. Heat Mass Transfer, **48** (2005)1107
[24] Einstein, A., Ann. Phys., **324** (2) (1906) 289
[25] Maiga, S. E., Nguyen, C. T., Galanis, N., Roy, G., 2004. Super Lattices Microstruct. **35** 543
[26] N. Putra, W. Roetzel, S. K. Das, Heat Mass Transfer **39** (2003) 775
[27] Maxwell, J. C., *Electricity and Magnetism*, Clarendon Oxford, UK. (1873)
[28] Yu, W., Choi, S. U. S., 2003, J. Nanopart. Res., **5** (1) 167
[29] Xie, H., Fujii, M., Zhang, X., Int. J. Heat Mass Tran., **48** (14), (2005) 2926
[30] Sitprasert, C., Dechaumphai, P., Juntasaro, V., J. Nanopart. Res., 11(6), (2009) 1465
[31] Eastman, J., Choi, S. U. S., Li, S., Thompson, L., Lee, S., *Proceedings of the Symposium on Nanophase and Nanocomposite Materials II*, Materials Research Society, Boston, **457** (1997) 3
[32] Patel, H., Sundararajan, T., Das, S., 2010, J. Nanopart. Res., **12** (3), 1015
[33] Bruggeman, D. A. G. Annalen der Physik, Leipzig, **24** (1935) 636
[34] Hamilton, R. L., Crosser, O. K., 1962 Ind. Eng. Chem. Fund., 1(3), pp. 187
[35] Das, S. K., Putra, N., Thiesen, P., Roetzel, W., ASME J. Heat Transfer, **125** (2003) 567
[36] Chon, C. H., Kihm, K. D., Lee, S. P., Choi, S. U. S., Appl. Phys. Lett., **87** 15 (2005) 153107.
[37] Koo, J., Kleinstreuer, C., J. Nanopart. Res., **6** 6 (2004) 577
[38] S. K. Das, N. Putra, P. Thiesen, and W. Roetzel, J. of Heat Transfer, Vol. **125** (2003) 567
[39] Seok Pil Jang, *et al.* Appl. Phys. Lett., Vol. **84**, No. 21 (2004)
[40] Shuichi Torii, Proceedings of international on EcoTopia Science, ISETS07 (2007)
[41] Shuichi Torii, 2-39-1 Kurokami, Kumamoto **860** (2009) 8555